Optimal Transition from Entry to Cruising Flight

ROBERT F. STENGEL*
Massachusetts Institute of Technology, Cambridge, Mass.

Following a high angle-of-attack (α) "blunt body" entry from orbit, the space shuttle orbiter will rotate to a low α for flight to an airport and a conventional aircraft landing. It is likely that the transition trajectory will carry the vehicle through a region of aerodynamic instability at intermediate α. Transition trajectories which minimize operation within the unstable region through the use of a subsonic jump maneuver are investigated here. Angle-of-attack penalties shape the control profile, which otherwise minimizes load factor while meeting terminal state conditions. Using a steepest-descent algorithm, the intermediate-α penalty is suppressed for the first several iterations, allowing the minimum load trajectory to be established. Increasing weighting on this penalty during succeeding iterations forces the control into the stable regions at higher and lower angles. These regions are then connected by a rapid (but continuous) jump through the unstable region. Numerical results for a straight-wing shuttle vehicle are obtained, including solutions for variations in initial and final conditions and for a range of lift/drag ratios and wing loadings. Small initial condition measurement errors are shown to be stable, and two forms of near-optimal control are considered.

Introduction

THE space shuttle orbiter will return to Earth on a trajectory which can be separated into three distinct flight regimes. The lifting hypersonic atmospheric entry will occur at high angle of attack, in order to provide in-plane and crossrange maneuverability, low deceleration, and low heating rates. Prior to landing, the vehicle will fly subsonically at low α, maneuvering as an aircraft in cruising flight and runway approach. Although many questions of control remain to be answered, the modes of trajectory and attitude control are fairly well-defined in these phases. During entry, the lift vector is rotated by reaction control thrusters to null landing point error, whereas in the latter case, aircraft practice can be followed. The third phase, the transition from entry to cruising flight, is less well understood. It possesses elements of both these flight conditions and involves rapidly changing dynamical parameters.

The principal requirement of the transition maneuver is that it provide a continuous link between entry and cruise while meeting the operational constraints of the mission, the vehicle, and its passengers. This must be accomplished for a variety of initial conditions, in the presence of state measurement uncertainties, and with high reliability. Total energy should be managed so that cruise range, with or without auxiliary air breathing propulsion, is maximized.

Aerodynamic instability is a fundamental problem of the transition phase. It is possible that the transition trajectory will carry the shuttle vehicle through a region where attitude motions would diverge in the absence of a stability augmentation system. Examples of such regions include the lateral-directional instability of the X-15 at α above 20°,[1] the well-known yaw-roll coupling of lifting bodies in transonic flight,[2] and the subsonic, longitudinal, pitch up instability of high aspect ratio designs.[3]

Numerical simulations of transition trajectories are an aid to understanding the maneuver, but the number and variety of boundary conditions and mission constraints preclude effective use of an experimental, open-loop approach to trajectory shaping. Optimal control methods reduce the guesswork in design, affording a consistent framework for generating and evaluating control strategies. Optimality, in the sense of minimizing time or fuel, is not a goal of the present study. The energy necessary for control is small, and the time available for the maneuver is open.

What is optimized is the terminal state error, subject to penalties on load factors other than 1 and on operation within unstable regions (in this case, defined by the control only). The tolerance on the desired terminal state, cruise velocity and flight path angle at a given altitude, is large, as the shuttle can adjust to a wide range of cruise flight conditions by manipulating α; hence, some terminal error is allowable, and there is no need for a hard terminal constraint. The control penalty demonstrated here establishes two acceptable (stable) regions of control for each point on the trajectory with an unacceptable (unstable) region separating them. Since the unstable region must be traversed, it is done so only once, and the control profile follows local minima at all other times.

The problem posed for this paper is the transitional control of velocity, flight path angle, and altitude through aerodynamic forces, using α as the control variable. Range is open, and rotational dynamics are not considered; thus, terminal navigation and stability augmentation are not addressed. After presenting the equations of motion and the steepest-descent optimization equations, numerical results for a typical shuttle vehicle are obtained. Solutions for a variety of initial conditions, final conditions, and vehicle parameters are given, and the effects of some initial condition measurement errors are noted.

Dynamics

The equations of motion are written for a vehicle free to translate in planar motion about a spherical, nonrotating Earth of radius R. The angle of attack α is measured between the velocity vector (whose magnitude and angle down from the local vertical are x_1 and x_2) and the vehicle centerline. Altitude above the Earth's surface is x_3 and range from some initial point is x_4. The nonlinear dynamical equation of the state vector $\mathbf{x}$ is

$$\dot{\mathbf{x}} = \mathbf{f}(\mathbf{x},\alpha,t), \tag{1}$$

Received August 11, 1970; presented as Paper 70-1018 at the AIAA Guidance, Control and Flight Mechanics Conference, Santa Barbara, Calif., August 17–19, 1970; revision received June 16, 1971. This research was supported by NASA Contract NAS 9-10268.

* Leader, Atmospheric Flight Mechanics and Entry Control Group, Apollo Guidance and Navigation Program, Charles Stark Draper Laboratory. Member AIAA.

where

$$f_1 = -D/M - g\cos x_2 \quad (2)$$

$$f_2 = [g/x_1 - x_1/(R + x_3)]\sin x_2 - L/mx_1 \quad (3)$$

$$f_3 = x_1\cos x_2 \quad (4)$$

$$f_4 = x_1\sin x_2/(1 + x_3/R) \quad (5)$$

For the transition maneuver, the mass m is assumed constant. The drag and lift forces D and L are functions of the state through the intermediate variables, Mach number M and dynamic pressure q

$$L = C_L(\alpha,M)Sq \quad (6)$$

$$D = C_D(\alpha,M)Sq \quad (7)$$

$$M = x_1/a(x_3) \quad (8)$$

$$q = \rho(x_3)x_1^2/2 \quad (9)$$

Density ρ and sound speed a are tabulated functions of altitude taken from the 1962 U.S. Standard Atmosphere,[4] and gravity is inversely proportional to the Earth radius magnitude

$$g = g_R/(1 + x_3/R)^2 \quad (10)$$

Linear interpolation has been used for points between the tabulated values of C_L, C_D, α, and a, whereas an exponential interpolation is used for ρ. A Runge-Kutta algorithm with variable time step is used to integrate Eq. (1).

Optimization Equations

A steepest-descent method, which follows Bryson and Ho,[5] has been used to find the local optimal control profile, $\alpha(t)$. The object of the optimization is the minimization of the cost function,

$$J = (\mathbf{x} - \mathbf{x}_c)^T\mathbf{Q}(\mathbf{x} - \mathbf{x}_c) + \int_{to}^{tf}[\mathfrak{L} + \boldsymbol{\lambda}^T(\mathbf{f} - \dot{\mathbf{x}})]dt \quad (11)$$

where $\mathbf{x}_c$ denotes the cruise condition at the terminal altitude, x_{3f}. For near-horizontal flight ($\gamma \simeq 0$) and the velocities of interest (<3500 fps), the cruise velocity x_{1f} satisfies the equation,

$$C_L(\alpha,M)Sq/mg = 1 \quad (12)$$

where C_L is chosen to yield maximum lift/drag ratio, and M and q are defined by Eq. (8) and (9). For powered cruising flight, $\gamma = 0$, and $x_{2f} = \pi/2 - \gamma = \pi/2$. For an unpowered equilibrium glide,

$$x_{2f} = \pi/2 + \tan^{-1}(D/L) \quad (13)$$

The weighting matrix $\mathbf{Q}$ is a diagonal matrix chosen to equate error variances of the final state variables, i.e., to establish the tradeoffs between velocity, angle, and altitude which are acceptable at the transition's final time. Except as noted, $\mathbf{Q}$ places equal weights on standard deviations of 5 fps, 1 deg, and 200 ft – altitude, with no consideration given to range (x_{4c} is unspecified and $q_{44} = 0$). The Lagrangian $\mathfrak{L}$ is composed of two parts. $\mathfrak{L}_1$ assesses penalties to load factors other than 1 and is

$$\mathfrak{L}_1 = k_1[(C_L^2 + C_D^2)^{1/2}Sq/m - g]^2 \quad (14)$$

The control penalty $\mathfrak{L}_2$ has continuous first derivatives but is functionally separated into five α regions. There are quadratic penalties for exceeding the maximum and minimum boundaries of control α_0 and α_3 and there is an internal range of unacceptable angles between α_1 and α_2. $\mathfrak{L}_2$ is described by

$$\mathfrak{L}_2 = \begin{cases} k_2(\alpha - \alpha_0)^2 & \alpha < \alpha_0 \\ 0 & \alpha_0 \le \alpha \le \alpha_1 \\ k_3(n)\sin^2\pi\left(\dfrac{\alpha - \alpha_1}{\alpha_2 - \alpha_1}\right) & \alpha_1 < \alpha < \alpha_2 \\ 0 & \alpha_2 \le \alpha \le \alpha_3 \\ k_4(\alpha - \alpha_3)^2 & \alpha < \alpha_3 \end{cases} \quad (15)$$

$k_3(n)$ is a weighting factor which is dependent on the number of iterations in the optimizing process. The sine-squared term erects a barrier between the acceptable control regions $[\alpha_0,\alpha_1]$ and $[\alpha_2,\alpha_3]$; therefore, it is suppressed until a trajectory minimizing end-state error and the time integral of $\mathfrak{L}_1$ is obtained. Once a suitable control in $[\alpha_0,\alpha_3]$ is found, the penalty on control in (α_1,α_2) grows, forcing $\alpha(t)$ to take values in the acceptable regions. In the current example,

$$k_3(n) = 0 \qquad ,n < m \quad (16a)$$

$$k_3(n) = C_1(n - m)^2/(n - m)^2 + C_2 \qquad ,n > m \quad (16b)$$

The optimization is an iterative process, beginning with the forward integration of Eq. (1), using an initial guess for the control profile. The adjoint equation,

$$\dot{\boldsymbol{\lambda}} = -\mathbf{f}_x^T\boldsymbol{\lambda} - \mathfrak{L}_x^T \quad (17)$$

is integrated from t_f to t_o, using partial derivatives tabulated during the state integration and the starting conditions (at t_f),

$$\lambda_i(t_f) = 2q_{ii}(x_i - x_{ci}), \quad i = i,4 \quad (18)$$

Having obtained a time history of $\boldsymbol{\lambda}$, the control for the next forward integration is perturbed by

$$\delta\alpha(t) = -k_5(\mathfrak{L}_\alpha + \boldsymbol{\lambda}^T\mathbf{f}_\alpha)^T \quad (19)$$

The final time for the next state integration is modified by the relation

$$\Delta t_f = -k_6\left[\left(\frac{\phi_f - \phi_{f-1}}{t_f - t_{f-1}}\right) + \mathfrak{L}_f\right] \quad (20)$$

where the ϕ's are the weighted terminal state error variances at the final time and the previously tabulated time, t_f and t_{f-1}. For a given run, the tabulation time increment is fixed (at 2 seconds), and final time perturbations are rounded to multiples of the time increment. For $\Delta t_f > 0$, $\alpha(t)$ is fixed at the last computed value.

In the numerical results which follow, the choice of the k_i has been governed by considerations of linearity and convergence. Eqs. (17) and (19) predicate linear perturbations about a reference state and control. The lift and drag control forces meet this criterion only for small angle-of-attack changes, and k_5 is chosen accordingly. k_6 is a saturation element limiting Δt_f to one or two time increments. This is made necessary by the sensitivity of all three state components to changes in final time. k_1 attenuates the load factor penalty, allowing angle-of-attack penalties to dominate the control perturbation and terminal errors to control the final time variation.

Vehicle Model

The straight-wing orbiter proposed by Faget[3] is taken as a prototype for the transition study. The vehicle is assumed to weigh 164,000 lb and to have a wing area of 1850 ft,^{2} resulting in a wing loading (W/S) of 89 psf.

One form of instability which can occur within the control range and which cannot be avoided in a subsonic transition from high to low angle of attack is a positive pitch moment coefficient slope at intermediate angles. Ref. 3 presents

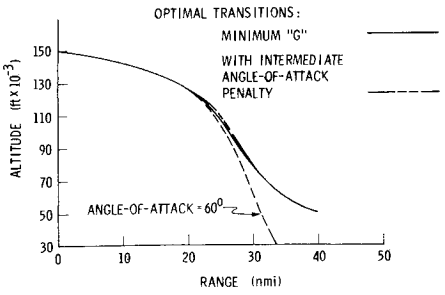

Fig. 1 Transition trajectories to an equilibrium glide at 50,000-ft altitude.

this case and further indicates that there is sufficient control power to break the high α, deep-stall equilibrium and to perform the transition.

At the time of this study, lift and drag coefficients were available only for hypersonic and low subsonic flight. These data provided adequate coverage of the α range, but gave no information concerning the transonic and supersonic regimes. It was necessary, therefore, to fill in the missing data using theoretical and empirical functions which strictly apply only to lift coefficients at low α.[6]

Under these assumptions, the maximum subsonic lift/drag ratio of 7.95, which occurs at $\alpha = 4°$, is independent of Mach number, and the trim flight path angle is $-7.16°$ for subsonic glide at $(L/D)_{MAX}$. The corresponding cruise velocities range from 508 to 860 fps (Mach numbers from 0.51 to 0.89) as cruise altitude increases from 30,000 to 60,000 ft. Glide range, which is proportional to L/D and starting altitude, increases from 39 to 78 nautical miles for this range of possible transition terminal conditions.

For the optimal paths of this study, the outer α penalties are established at 2° and 60°, while the unacceptable intermediate region lies between 20° and 50°.

Numerical Results

A typical orbital return trajectory begins at 400,000 ft, with a flight path angle of -1.5 deg and an Earth-relative velocity of 24,400 fps. Entering with positive lift and an α of 60°, the shuttle passes through Mach 3 (3203 fps) at an altitude of 150,000 ft; the flight- path angle is $-5.97°$.

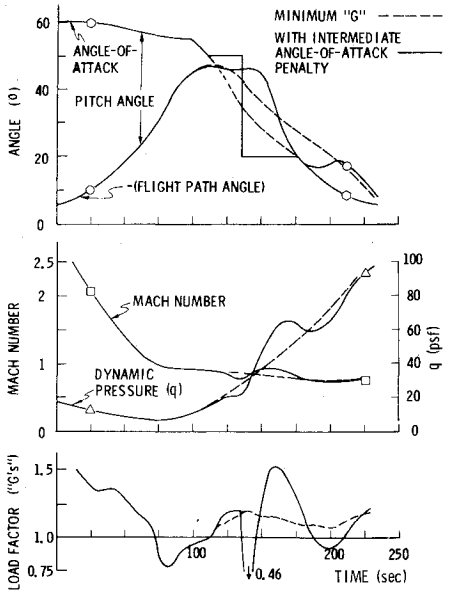

Fig. 2 Parameters of the transition trajectories.

Maintaining α at 60° would result in a subsonic L/D of 0.59 and a trim glide γ of $-59°$ as the spacecraft descended to Earth. The vehicle would have a near-horizontal pitch attitude θ in this stable deep-stall condition. It is necessary to dive sharply in order to avoid the unstable region, to capture a low-α equilibrium, and to pick up sufficient velocity for cruising flight (trading potential energy for kinetic energy). It is possible to "overspeed" during the dive, i.e., to exceed the vehicle's Mach limitation for low-α, high-dynamic-pressure (q) flight. This limitation also applies to the cruise condition and is the prime consideration in determining the terminal altitude of the subsonic transition maneuver.

Numerical examples of the effects of initial condition variations, final condition variations, transition duration, wing loading, subsonic L/D, initial condition measurement errors, and the range of the unstable region follow.

Nominal Transition

The nominal transition for this study begins at the Mach 3 point mentioned above and terminates at an altitude of 50,000 ft with velocity and γ of 733 fps and $-7.16°$. The Mach number is 0.76. Figure 1 compares the altitude-range profiles of optimal transitions (with and without the intermediate-α penalty) with the constant-α trajectory. The optimal paths first diverge from the constant-α path at an altitude of 125,000 ft, terminating in the 50,000-ft cruise condition.

Several parameters of the optimal transitions are plotted against time in Fig. 2. The control profiles are identical during the first 108 sec, at which point the constrained-α case fixes on the unstable region's upper boundary. The unconstrained, minimum load factor control decreases continuously to the end point. At 148 sec, the constrained control takes 2 sec to jump to the lower unstable region boundary, holding constant until meeting the unconstrained control at 182 sec. The mid-point of the jump (35°) coincides with minimum "g" control. Flight path angle also is plotted (with opposite sign) in Fig. 2a. Without the intermediate-α penalty, γ reaches a single minimum of $-47°$; the penalty forces a second minimum in the vicinity of the absolute minimum and a third near the final time. Since,

$$\theta = \alpha + \gamma = \alpha - (-\gamma), \tag{21}$$

the difference between the α and γ curves of Fig. 2a defines the spacecraft's attitude with respect to the local horizontal. Both trajectories begin with the vehicle pitched up 54°.

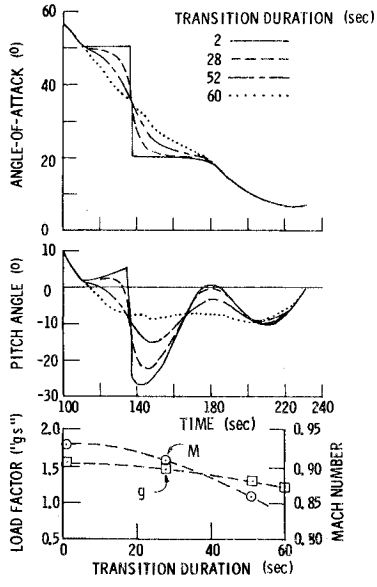

Fig. 3 Effects of transition jump duration on flight parameters.

The attitude is horizontal at 114 sec and dips 9° below the horizontal before coming to a −3° equilibrium at the end of the unconstrained transition. In the second case, the α penalty forces the vehicle to remain pitched up until the time of transition. The α jump requires a pitch change of −30°, and θ reaches minima of −27° and −10° on the constrained trajectory.

Figures 2b and c indicate that the α jump superimposes oscillations on other parameters as well. The Mach number oscillation is of most concern; a peak of 0.93 is reached while at an α of 20° and a dynamic pressure of 54 psf. It will be seen that this peak always occurs and that its value diminishes with increasing jump duration and decreasing altitude. Load factor reaches a relative maximum of 1.53 during the transition. This is less than the maximum (1.9) during entry.

Transition Duration Effects

In the previous section, (and in later sections), the intermediate-α penalty is large enough to force a 2-sec angle-of-attack jump. Reducing the penalty allows a more gradual transition, with accompanying reductions in maximum load factor and low-α Mach number. Defining the transition duration as the time required for α to drop from 49° to 21°, the 2- and 60-sec cases of Fig. 3 correspond to the nominal jump and minimum-load-factor cases of the previous section. This figure shows that θ excursions decrease as transition duration increases and that θ is predominantly negative during the transition. In addition to lessening the post-jump Mach rise and maximum load factor, a gradual transition is more realistic than the 2-sec maneuver, for the spacecraft possesses inertia and limited control power. Furthermore, when rotational dynamics are considered, the abrupt maneuver constitutes a larger input to the short period mode, with the possible result of increased attitude, load factor, and Mach number overshoot. The choice of transition duration is thus affected not only by the moment instability but by the transient response as well. (A separate report[7] indicates that such overshoots can be controlled if the jump maneuver is forced by an elevator doublet. As jump duration is decreased, elevator rate and deflection range increases. Slower transitions ease this problem but increase the need for a stability augmentation system.)

Variations in Final Altitude

For the assumed vehicle model, subsonic cruise equilibrium can be achieved up to altitudes greater than 60,000 ft. End points from 30,000 to 60,000 ft have been examined at 10,000-ft intervals, each having a γ of −7.16° and the appropriate cruise velocity. Difficulty in end-point convergence was experienced for the 60,000-ft case, where terminal corrections were made at transonic velocities and where coefficient variations from point to point were large. As a result, altitude error is 250 ft, and velocity/γ errors oscillate between 10 fps/3.3° and 30 fps/1.6° on succeeding iterations.

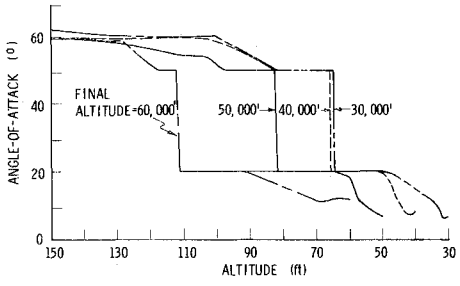

Fig. 4 Angle-of-attack profiles for transition to several final altitudes.

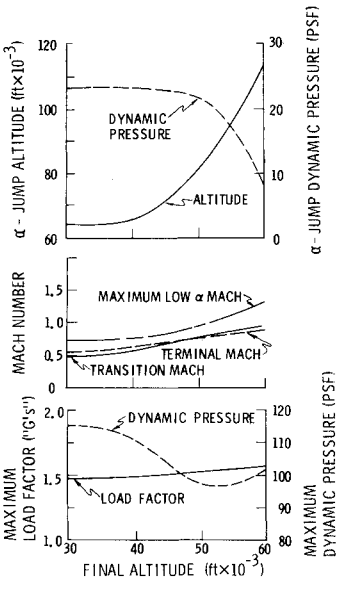

Fig. 5 Effects of final altitude on flight parameters.

Angle-of-attack profiles for the four cases are shown in Fig. 4. All begin in the vicinity of 60°, drop to the 50° upper boundary, jump to the 20° lower boundary, and vary to null end point error. The high-altitude control profiles are sensitive to final time. The 2-sec uncertainty imposed by the quantized final time adjustment causes variations of 1° to 2° in the 50° to 60° region. This has small effect on terminal error, as the local lift-slope is low, changes in load factor are therefore small, and the optimal control is stable. Variations in the low-altitude control profiles arise from the Mach-dependence of aerodynamic coefficients.

The altitudes at which the control jumps are initiated are shown in Fig. 5a. Together with dynamic pressure, load factor, and Mach number, transition conditions appear similar in the 30,000- to 40,000-ft range. Jump altitude and M increase with final altitude, and q decreases. As indicated by Fig. 2b, M reaches a maximum after the jump; Fig. 5b shows that this maximum increases with the target altitude. In Fig. 5c, maximum load factor changes little with final altitude, and maximum dynamic pressure is hardly larger than that necessary for cruise (115–83 psf for increasing altitude).

Variations in Final Flight Path Angle

The principal differences between trajectories with trim-glide and near-zero flight path angles are the α-jump altitude and the V, α, and γ during the last 30 sec of the transition. Targeting on zero γ(−1.63° was achieved), the jump

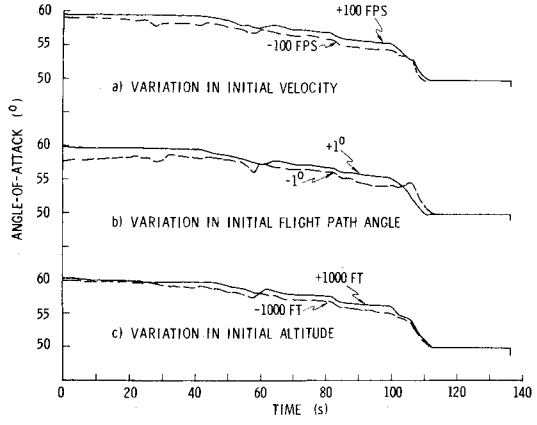

Fig. 6 Variations in angle-of-attack profiles caused by known changes in initial conditions.

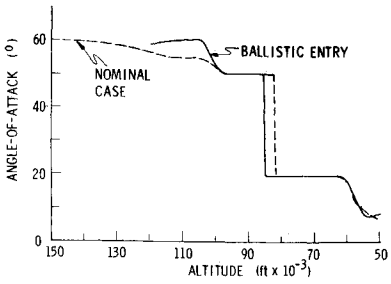

Fig. 7 Comparison of angle-of-attack profiles for nominal and ballistic entry initial conditions.

occurs 5000 ft lower than on the nominal control, incidentally reducing the maximum low-α Mach number of 0.88. In order to achieve horizontal flight at the cruise velocity, an additional 30 fps is maintained, and a steeper pullout is performed in the last 16 sec.

Known Initial Condition Variation

Perturbations to the initial state produce their most significant effects in the control profile prior to the α jump. For the cases considered (± 100 fps, $\pm 1°$, ± 1000 ft), the time for the jump is unchanged. As listed in Table 1, variations of V and γ from nominal are small at jump time. Altitude variations at jump time are large because it is an integral of V and γ, and close control of the latter is more important to the minimization of the state error.

The α profiles are plotted in Fig. 6. The point-to-point variation is a predictable phenomenon of the steepest descent algorithm and is not significant. Differences in control for the velocity perturbation are spread evenly over the time interval. Differences for γ perturbations are larger in the early portion, and they are larger at the later times for altitude perturbations.

The particular importance of early flight path control is emphasized by the ballistic case, whose initial conditions are representative of a rolling entry from orbit in which net lift is cancelled up to the beginning of transition. This case also is similar to an early abort; the Mach 3 point is entered with the steep angle of $-15.9°$ at an altitude of 120,000 ft. The load factor here is 5.6. The altitude profile of control is compared with the nominal case in Fig. 7. The ballistic and nominal controls reach the 50° boundary and leave the 20° boundary at nearly identical altitudes. As indicated by Table 1, the jump altitudes are 3819 ft apart; and the flight path angles differ by just 1°. Referenced to the Mach 3 starting time, the α jump is 54 sec earlier on the ballistic transition.

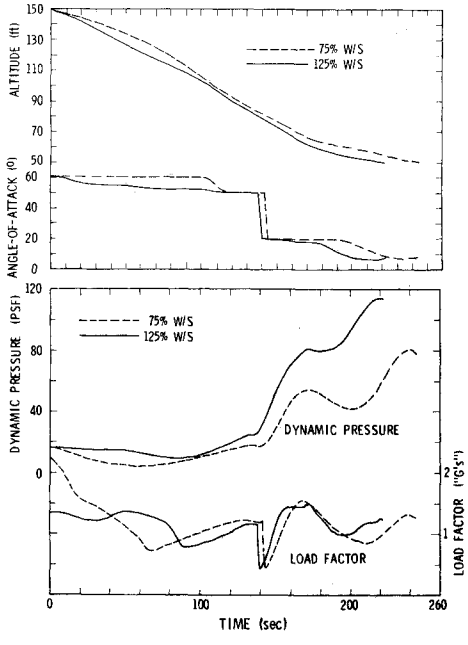

Fig. 8 Effects of wing loading on altitude, angle of attack, dynamic pressure, and load factor.

Unknown Initial Condition Variations

In the previous case, it was assumed that the initial state perturbations were measured exactly. New control profiles were computed, giving examples of control sensitivity. If, on the other hand, the perturbations are not measured and it is assumed that the initial conditions are nominal, what is the effect of the nominal control on terminal state error?

Terminal state errors for desired final altitudes of 30,000 and 50,000 ft appear in Table 2. Keeping in mind that a positive (unknown) variation is a negative measurement error, it can be seen that the flight path is stable. Errors of like kind decrease between initial and terminal times, and errors for the 30,000-ft case are smaller than those of the 50,000-ft case. Seckel[6] provides a simplified, quasi-steady equation governing V,γ perturbations about steep trajectories. With a change of notation, the characteristic equation is,

$$p^2 + (C_D - W\sin\gamma/2Sq)p + [(C_L + W\cos\gamma/Sq)\cos\gamma - C_D\sin\gamma](W/2Sq) = 0 \quad (22)$$

where p is the operator, $d(\ )/d(\rho SVt/m)$. Although the quasi-steady description is not valid for extended segments of the trajectory, it is clear that Eq. (23) is stable about all working points of the transition, since γ is negative and both coefficients of the equation are always positive.

Wing Loading Effects

For the given set of initial conditions and a 50,000-ft final altitude, changes to the spacecraft's wing loading, W/S, produce several interesting effects in the transition trajectory. The trim-glide γ is unchanged, as it is a function only of $(L/D)_{MAX}$, but the corresponding velocity for unity load factor must vary. Reducing W/S to 75% of the nominal (89 psf) value reduces the cruise velocity from 733 to 656 fps, while increasing W/S by 25% raises the velocity to 793 fps.

The control profiles are quite different, as the lighter vehicle stays at 60° for over 100 sec and the heavier vehicle begins to lower its angle almost immediately. It is surprising, then, that the jump altitudes are only 442 ft apart. Figure 8a provides this information and also indicates that altitude rate is relatively constant until α leaves the lower unstable boundary. Dynamic pressure profiles are similar up to the jump, at which time they begin to adjust to their cruising flight values (see Fig. 8b). From 90 sec on, load factors are very nearly equal in magnitude, differing up to 20 sec in timing. In both cases the minimum pitch angle is $-28°$.

Table 1 Effects of known initial condition variations on flight parameters at final time and transition jump time

Initial Condition Perturbation	Δx_{1f}, fps	$\Delta\gamma_f$, deg	Δx_{3f}, ft	$\Delta\gamma_2$, deg jump	$\Delta\gamma_2$, deg jump	Δx_3, ft jump
+100 fps	−0.1	−0.2	39.0	5.2	−0.3	205.0
−100 fps	1.1	−0.4	−43.0	−7.1	0	−551.0
+1°	0.1	0.3	29.0	9.2	−0.3	461.0
−1°	−0.1	0.4	−20.0	−7.8	−0.2	−574.0
+1000 ft	−0.1	0.2	−25.0	−5.0	−0.3	−537.0
−1000 ft	0.1	0.3	27.0	−8.0	0.1	−806.0
"Ballistic" (−92 fps, −9.9 deg, −30,000 ft)	0.72	−0.2	97.0	46.0	−1.0	3819.0

Lift/Drag Effects

Optimal transitions have been obtained for arbitrary variations of +50% and −25% in subsonic C_L, resulting in lift/drag ratios of 11.93 and 5.96; supersonic L/D was unchanged. A direct consequence of the L/D variation is that terminal state cruise conditions are modified. Cruise velocities for the high and low L/D become 625 and 810 fps, while the trim-glide flight path angles are −4.79 and −9.5°. The transonic cruise Mach number for the low L/D case (M = 0.84) produces the convergence difficulty mentioned earlier in connection with a 60,000-ft terminal altitude. As shown in Fig. 9, M rises to 1.3 after the α jump for this case. This figure also indicates the qualitative differences due to L/D variation, particularly the variation in α jump altitude, the divergence of dynamic pressure profiles to account for desired terminal conditions, the lack of significant Mach rise in the high L/D case, and the 74 sec difference in flight times during the transition. Using Eq. (22), Fig. 9a indicates that θ profiles are also substantially different: although both are oscillatory after the jump, the low L/D pitch angle is always negative, while the high L/D angle has a positive peak. As might be expected, the post-jump load factor is lower at high L/D reaching a maximum of 1.51 compared to 1.7 for the low L/D case.

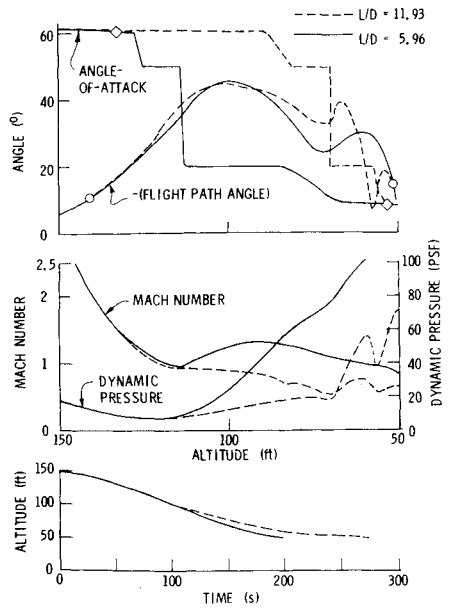

Fig. 9 Effects of lift-drag ratio on angle of attack, flight-path angle, Mach number, dynamic pressure, and altitude.

Near-Optimal Control

Three reasons for consideration of near-optimal α profiles are greater simplicity, control sensitivity, and low-α Mach limitation. If, for example, the 60° entry angle of attack can be maintained up to the transition's jump, trajectory control is simplified (although the elevator deflection profile required to produce the α-profile may be complex[7]). In obtaining numerical results for the previous cases, it was noted that control before the α jump is very sensitive to terminal time, yet post-jump control is capable of nulling terminal errors for a wide range of terminal times. If the low-α Mach limitation is exceeded in the post-jump dive, it is necessary to reshape the control profile. An additional penalty, perhaps of the form,

$$\mathfrak{L}_3 = k_c(\alpha_2 - \alpha)^2(M - M_0)^2,\ \alpha < \alpha_2,\ M > M_0 \quad (23a)$$

$$\mathfrak{L}_3 = 0, \text{ otherwise} \quad (23b)$$

could be considered; however, upon consideration of the topology of ($\mathfrak{L}_2 + \mathfrak{L}_3$), it is easy to see that local minima which violate $\mathfrak{L}_2$ and $\mathfrak{L}_3$ separately are formed and could confound the minimization.

The first near-optimal control to be considered is the constraint of pre-jump α to 60° by extending the upper boundary of the intermediate penalty region to 60°. Transition trajectories are obtained as before and are nonoptimal only in the sense that the penalty region is greater than the unstable region of control. This strategy will be called high-α constraint control.

The control profiles which result are shown in Fig. 10 (the 60,000-ft terminal altitude case has been excluded). Comparing this figure with Fig. 4, the α jumps are seen to occur a few thousand feet above their counterparts. This is caused by the greater deceleration at the higher α and by the shift in the unacceptable region's midpoint to 40° (which determines jump time from the unconstrained optimal control). Overlaying the two figures reveals that the control profiles for given final altitudes leave the lower penalty region boundary at virtually identical altitudes. The undershoots occurring after two of the jumps are thought to be artifacts of the steepest-descent algorithm.

There is little that is different about the resulting trajectories. Changes to the maximum dynamic pressures (see Fig. 5) are negligible, and maximum load factors increase about 7%. Maximum Mach numbers increase from 0.03 to 0.05, a matter for concern in the 50,000-ft case. The minimum θ decreases 9°, i.e., becomes steeper. For comparison of α, γ, and θ, with Fig. 2, a similar plot is given in Fig. 11. Flight path angles have similar contours in both cases, but reach more negative values in the near-optimal case. Pitch attitude is positive up to the jump and again near 180 sec.

A pragmatic, if nonoptimal, solution to the Mach limitation problem is to delay the jump time of the high-α constraint control, optimizing only the low-α control. The jump is then initiated at a lower Mach number, and a greater increase is needed to reach the limit.

An example with jump time delayed by 20 sec is considered. Referring to Fig. 11, the delayed jump trajectory stays with the α = 60° reference case down to an altitude of 74000 ft and 0.61 Mach number. Following the jump, the 50,000-ft cruise condition is reached at a range of 35.3 nmi, and the maximum low-α Mach number is 0.85. The Mach rise

Table 2 Effects of unknown initial condition variations on flight parameters at 2 terminal conditions

	50,000-ft Terminal Altitude			30,000-ft Terminal Altitude		
Measurement Error	Δx_{1_f}, fps	$\Delta\gamma_f$, deg	Δx_{3_f}, ft	Δx_{1_f}, fps	$\Delta\gamma_f$, deg	Δx_{3_f}, ft
−100 fps	5.8	0.1	469.0	2.5	0.1	275.0
+100 fps	−5.1	0.1	−411.0	−2.5	0.1	−271.0
−1°	7.9	0.1	636.0	3.5	−0.1	397.0
+1°	−7.1	0.1	−570.0	−3.6	0.1	−394.0
−1000 ft	3.0	0.1	252.0	1.4	0.0	151.0
+1000 ft	...	...	...	−1.4	0.1	−210.0

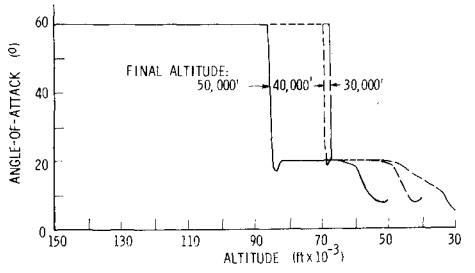

Fig. 10 Angle-of-attack profiles for high α constraint control.

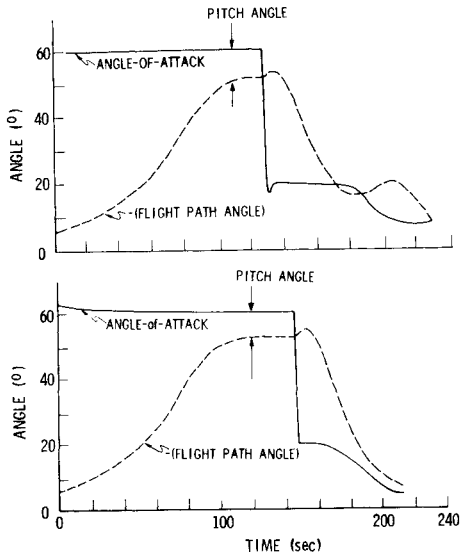

Fig. 11 Flight angles for a) high α constraint control and b) high α constraint control with jump time delayed by 20 sec.

is 0.24 (compared to the nominal 0.17), but there is a net decrease of 0.09 in the maximum Mach number. During the pull-up, the minimum θ is $-35°$ and load factor reaches a maximum of 1.62. Terminal errors are 0.7 fps, 0.1°, and 386 ft. In Fig. 11b, it can be seen that α actually began at 63° in this case; this could have been corrected by a choice of greater stop time for the starting iteration or by additional iterations. Unlike the previous case, there is no oscillation in γ after the jump, and pitch angle stays negative after the transition to low angle of attack.

Conclusions

Transition trajectories connecting the entry and cruising phases of a lifting vehicle's return from orbit are readily studied using optimal control. The consistent framework for analysis of state and parameter variations is essential, as prior art does not provide satisfactory comparisons.

A Mach 3 starting point was chosen for the investigation to eliminate heating constraints yet allow ample time for optimal maneuvers. Assuming a subsonic cruise terminal condition, it was found that a terminal altitude of 50,000 ft can be obtained without exceeding the speed of sound at low α, using a control profile which jumps through an unstable angle-of-attack region while minimizing load factor. The time spent within the unstable region is controlled by assessing a penalty to the range of α for which the instability occurs. For the assumed vehicle model, transition to a 60,000-ft altitude requires a return to supersonic speed at low α, and convergence to the 0.89 Mach number cruise condition is complicated by the transonic compressibility rise in C_L and C_D.

Although shaping of the α profile prior to the transition jump is an aid to end state and load factor control, a high-α constraint control is nearly as effective. It appears that optimal control after the jump is sufficient for a range of initial conditions, and that varying jump time either in an optimal or empirical fashion, provides additional control of end state and maximum low-α Mach number.

References

[1] Taylor, L. W., Jr., Merrick, G. B., "X-15 Airplane Stability Augmentation System," NASA TN D-1157, March 1962 NASA.

[2] Steketee, F. D., "Dynamic Stability of Space Vehicles, Vol. XI, Entry Disturbance and Control," CR-945, Nov. 1967, NASA.

[3] Faget, M., "Space Shuttle: A New Configuration," *Astronautics and Aeronautics*, Vol. 8, No. 1, Jan. 1970, pp. 52–61.

[4] U.S. Standard Atmosphere, 1962, U.S. Government Printing Office, Washington.

[5] Bryson, A. E., Jr., Ho, Y. C., *Applied Optimal Control*, Ginn-Blaisdell, Waltham, Mass., 1969.

[6] Seckel, E., *Stability and Control of Airplanes and Helicopters*, Academic Press, New York, 1964.

[7] Stengel, R. F., "Space Shuttle Transition to Cruising Flight," Rept. E-2539, Sept. 1970, Charles Stark Draper Lab., MIT, Cambridge, Mass.